Preprint Cambridge Centre for Computational Chemical Engineering ISSN 1473 – 4273

Surface reactivity of homogenous polycyclic aromatic hydrocarbon nano-clusters

Dongping Chen [1], Jethro Akroyd [1], Sebastian Mosbach [1], Markus Kraft [1]

released: 24th December 2013

[1] Department of Chemical Engineering
and Biotechnology
University of Cambridge
New Museums Site
Pembroke Street
Cambridge, CB2 3RA
United Kingdom
E-mail: mk306@cam.ac.uk

Preprint No. 139

Keywords: Surface reactivity, PAH, nano-cluster, pocket, alpha

Edited by
Computational Modelling Group
Department of Chemical Engineering and Biotechnology
University of Cambridge
New Museums Site
Pembroke Street
Cambridge CB2 3RA
United Kingdom

Fax: + 44 (0)1223 334796
E-Mail: c4e@cam.ac.uk
World Wide Web: http://como.cheng.cam.ac.uk/

Abstract

A scheme to characterise surface atoms is proposed to probe molecular representations of homogenous pyrene and coronene clusters. The concept of solvent-excluded surface, which is widely used for proteins, forms the basis of this scheme. The scheme is used to provide insights into the surface reactivity in terms of the surface availability of active atoms and sites for different gaseous species. It was found that the surface availability of active sites varies with gaseous species, system temperature and particle size. The number of active sites available for a small gaseous species is always greater than that for a large species. Surface exposure increases with an increase in temperature and an obvious enhancement exists when transforming to liquid-like configurations. The surface availability decreases with increasing particle size following a linear relation with reciprocal size. The upper bound of parameter α, which is used in the soot literature to empirically quantify surface reactivity, was further estimated from the surface availability of hydrogen atom in the context of HACA mechanism and was well below 0.1 for reactions between mature soot particles and acetylene. By exploring one particular pocket on the surface of a coronene cluster with 100 molecules, it was noted that it is feasible for both oxygen and acetylene molecules to penetrate inside the cluster. This fact indicates that the surface reactions occurring on particles are not limited to the actual boundary of the configuration but also certain regions beyond the boundary via surface pockets.

Contents

1 Introduction

Surface reactions play an important role in the mass growth of soot, and have been the subject of intense experimental and theoretical investigation [2, 14, 17, 20, 21]. However, these investigations are limited by poor understanding of the microscopic structure of soot. A surface reaction of a soot particle is defined as a reaction between a small gaseous species and an individual active site on the surface of soot particle [6, 26]. Usually, the aromatic sites in a particle are not always available for reaction [5]. A few reactive sites are "buried" inside the particle structure and not exposed to the gaseous species. This should be necessarily taken into account otherwise it will lead to overestimation of the surface availability of the sites and thus the rate of surface reaction. Experimentally, it is extremely difficult to probe this phenomenon because soot particles are structurally heterogeneous [28]. In contrast, Frenklach and Wang [12] proposed an empirical parameter, α, to account the availability of active sites which can react with gaseous species via the HACA mechanism. The main pathway of the HACA mechanism proceeds via the creation of surface radical sites by hydrogen abstraction, and later, the reaction of acetylene molecules with these sites to form 5- or 6-member rings. The growth processes can occur on the free-edge (FE), zig-zag (ZZ) and armchair sites of an individual PAH [22]. Surface oxidation reactions are also initialised by hydrogen abstraction at FE and armchair sites [1, 5].

Following Frenklach and Wang's initial investigation, more recent numerical studies have investigated the parameter α and applied it to understand the surface reactions of soot particles in laminar premixed flames [1, 14, 33, 34] and non-premixed co-flow flames [16, 25]. Likewise, a free model parameter known as growth factor g, is included in some population balance models to adjust the rate of surface reaction of PAHs in large soot particles [6, 26]. In nature, both parameters α and g represent a steric phenomenon that should be dependent on the microscopic arrangement of a soot particle. However, no one has yet estimated these parameters numerically due to the lack of a satisfactory microscopic representation. Recently, Chen and coworkers studied the thermostability of homogeneous pyrene and coronene clusters as analogues for nascent soot particles [8] and demonstrated a phase change due to the addition of mass [7]. These studies provide a representation of these particles that enables the theoretical investigation of their surface reactivity.

To enable the probing of a surface representation, Richards [18] first described a solvent-accessible surface (SAS) as the surface was traced out by the center of a spherical probe representing a solvent molecule of a defined size using a "rolling ball" algorithm [18] (see the dashed black line on Fig. 1). Later, a more appropriate concept, the solvent-excluded surface (SES), was proposed to represent the actual surface of a configuration [9] (see the orange solid line on Fig. 1). This surface contains the parts of the van der Waals surface of the atoms that are "touched" by the probe and linked by a series of concave and saddle-shaped surfaces between the atoms. In practice, the SES can be computed using a "rolling ball" algorithm [10, 23, 24]. Using the SES representation, reactive regions known as "pockets" can be identified inside a configuration [30]. Technically, a pocket inside a configuration is defined as an empty concavity on the surface of the configuration into which bulk gaseous or solvent atoms can gain access [19, 32]. In other words, a pocket

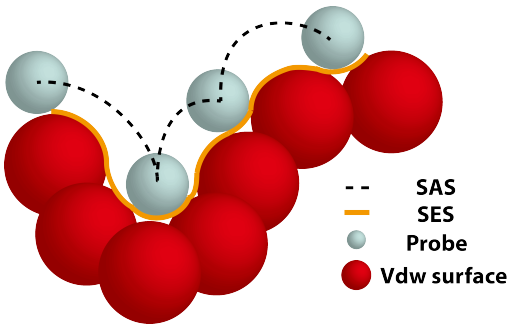

Figure 1: *Illustration of the "rolling ball" algorithm and the definition of the solvent accessible surface (SAS), the solvent-excluded surface (SES), and the van der Waals (Vdw) surface.*

represents a mouth-type opening connecting the interior with the outside atmosphere or solution. Obviously, pocket detection can geometrically characterise the surface porosity of a target configuration and thus we can investigate whether gaseous or solvent atoms can penetrate inside a configuration and react with the active sites via individual pockets.

In this work, the surface properties of homogenous pyrene and coronene clusters, including the surface availabilities of hydrogen atoms, FE and ZZ sites, are investigated microscopically using geometric analysis. For the first time, we can examine the surface reactivity of small PAH clusters directly from their molecular arrangements. We study the dependence of the surface availability on the gaseous species, system temperature and molecular size. We also identify surface pockets located on a particular particle and investigate whether gas-phase species can access regions beyond the boundary of the configuration of a coronene cluster via individual pockets.

2 Computational method

2.1 Molecular cluster

The current work investigates the surface reactivities of a number of nano-clusters, P_N. N denotes the number of molecules and varies from 50 to 500. P represents either pyrene or coronene. All the clusters were taken from previous work [8] in which the detailed microscopic representations were equilibrated using conventional Molecular Dynamics (MD). For each size, 100 different configurations have been extracted from a trajectory of 1 ns. The reported surface properties are computed by averaging over these configurations and the standard derivations are used to build the error bars.

The main concerns of this work are the surface availabilities of hydrogen atoms, FE and ZZ sites which determine the rates of surface reaction. There are 6 FE and 4 ZZ sites on a pyrene molecule, and 6 FE and 6 ZZ sites on a coronene molecule [4]. To identify the site types on the surface of microscopic representations, an index is assigned to each atom of the constituent pyrene and coronene molecules, such that the site type can be determined by analysing the atom indices.

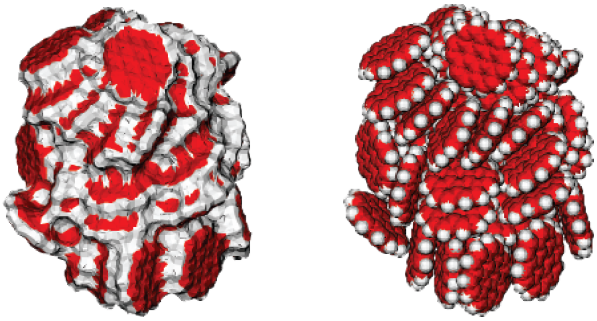

(a) *SES representation* **(b)** *Volumetric representation*

Figure 2: *Solvent-excluded surface (SES) and volumetric representation of a liquid-like coronene$_{50}$ cluster at 500 K. The red color represents the carbon atoms whilst the white color represents the hydrogen atoms. The solvent-excluded surface representation in Fig. 2a is generated using a probe with 0.17 nm radius, which is analogous to the size of a single carbon atom.*

2.2 Molecular surface analysis

Table 1: *Van der Waals radii for different gaseous species.*

Probe	radius (Å)
Hydrogen atom	1.2
Oxygen molecule[a]	1.52
Carbon atom	1.7
Acetylene molecule[b]	2.0

[a] *The size of the oxygen molecule is taken from the size of a single oxygen atom or half of its structure.*

[b] *The size of the acetylene molecule is taken from the length of a C-H fragment or half of its structure.*

SES was used to describe the molecular surface of the configurations in this work because it provides a more accurate description of the actual surface compared to that of SAS. The SES area was determined by the MSMS 6.2.1 program [27] which computes the surface area using a "rolling ball" algorithm. The radii of the carbon and hydrogen atoms are taken from their standard van der Waals radii as 1.7 and 1.2 Å respectively [3]. Fig. 2a shows a configuration approximated by SES using a spherical probe, whilst Fig. 2b illustrates the approximation of a configuration by representing atoms with solid spheres. Clearly, SES connects all the surface atom and forms a irregular molecular surface.

The contributions of each atom on the SES area can be calculated, and any atom with non-zero contribution is interpreted as a surface atom. The site information is obtained by analysing the indices of the surface carbon atoms. This characterisation of the surface atoms builds the basis of this work. We note that the characterisation is instantaneous and evolves in time as the molecules rearrange.

To enable the analysis of a target configuration, the surface availability of atom or site i, i_{surf}, is introduced to represent the availability of the active atom or site on a molecular

surface and it is computed by

$$i_{\mathrm{surf}} = \frac{S_{\mathrm{i}}}{N_{\mathrm{i}}}, \quad \text{where i} \in \{\text{hydrogen atom, FE and ZZ sites}\}. \tag{1}$$

S_{i} is the number of atoms or sites of type i accessible to a specific probe and N_{i} is the total number of atoms or sites of type i within the configuration. The physical representation of i_{surf} is the accessibility of atoms or sites of type i on the particle surface to the gas-phase species used as the probe. Thus, the surface accessibility to different gas-phase species can be estimated using a probe with a size corresponding to the size of a specific gas-phase molecule. This work considers four different-sized probes (Table 1) to represent the major gaseous species involving in the surface reactions of soot particles. As both oxygen and acetylene molecules are symmetrically linear molecules, the size of the oxygen and acetylene molecule is taken from half of their structures or one single oxygen atom and one C-H fragment respectively. It should be noted that i_{surf} may be interpreted as the upper bound of the parameter α for reactions involving atoms or sites of type i. The estimate is an upper bound because the calculation of i_{surf} assumes that gas-phase probe is able to freely access all surface atoms and sites.

2.3 Pocket detection

Surface pockets always act as pathways for gaseous molecules to gain access to the interior of a particle and represent the surface porosity of one particular particle. In this work, we used the pocket detection software package *Fpocket* [32], to identify pockets on the surface of homogenous PAH clusters and probe the corresponding surface porosity. This package was previously used in the characterisation of protein binding sites for ligand design [13] and it has been introduced in detail elsewhere [32]. Technically speaking, *Fpocket* performs a pure geometric analysis of the target configuration using the concept of alpha spheres (Fig. 3), introduced by Liang et al [19]. By definition, an alpha sphere is an empty spherical region that is bounded by the centres of four atoms within the cluster. By scanning the target configuration, an ensemble of different-sized alpha spheres can be identified, and an ensemble of pockets are identified from overlapping sets of alpha spheres. Note that it is necessary to impose upper and lower bounds on the allowed size of the alpha spheres. This is required to prevent the identification of large alpha spheres along the surface of the configuration and small alpha spheres throughout the configuration.

In this work, both carbon and hydrogen atoms were considered to bound the alpha spheres, whilst hydrogen atoms are usually ignored when investigating the surface of a protein [32]. The maximum allowed radius of the alpha spheres was 5 Å while the minimum radius was computed as the sum of the specific probe size and the radius of carbon which is 1.7 Å. For example, the minimum radius was 3.7 Å when using an acetylene molecule as the probe (Table 1). Such pockets are capable of accommodating at least one acetylene molecule and acting as a pathway allowing acetylene molecules physically to "touch" the interior of a configuration.

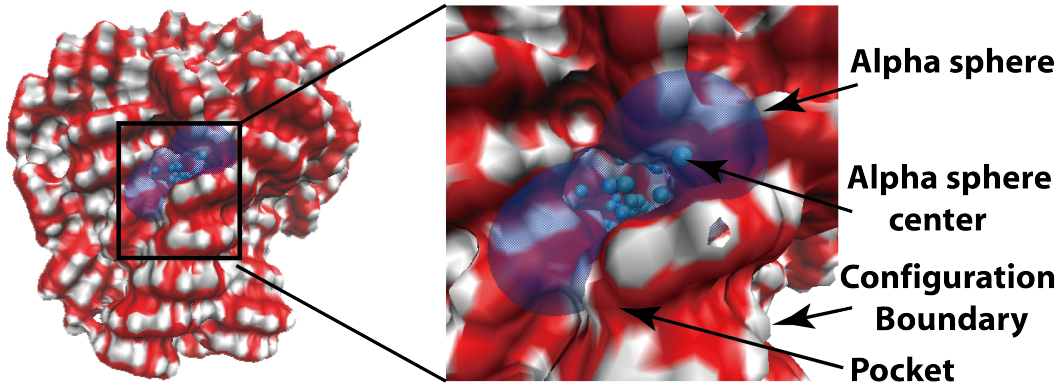

(a) *Front view*

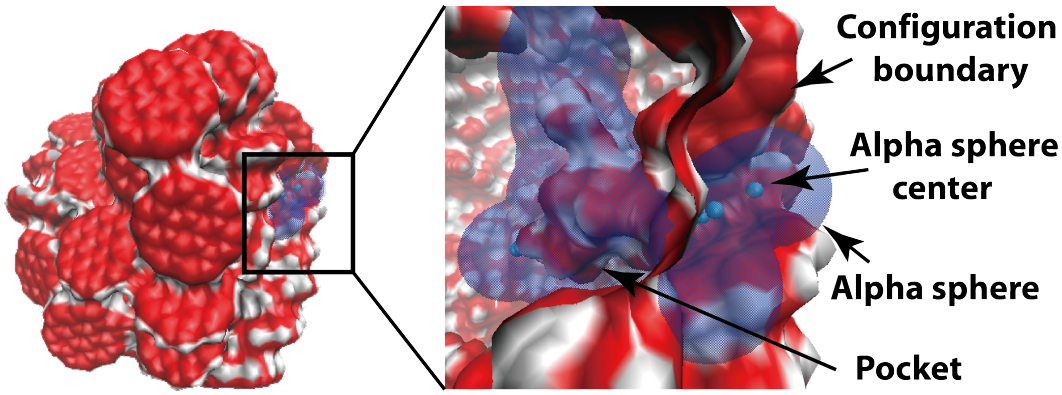

(b) *Side view*

Figure 3: *Illustrations of alpha spheres on a liquid-like coronene$_{100}$ cluster at 500 K using a probe with 0.12 nm radius. The solid light blue spheres represent the alpha sphere centers, and a set of the alpha spheres builds the transparent blue surface which is interpreted as a pocket using* Fpocket *[32]. The boundary of the configuration is highlighted to distinguish the inside of the configuration from the outside environment.*

3 Results

3.1 Probe dependence of the surface availability

Fig. 4 shows the surface availabilities of hydrogen atoms, FE and ZZ sites sites as a function of probe size. The surface availabilities decrease with increasing probe size. When the size of probe is less than 0.6 Å, the reported surface availabilities approach unity. However, as no species have such a small size (Table 1), this suggests that no molecule can move unrestricted within the configuration. When increasing the probe size, the reported surface availabilities asymptote as probes cease to pick out the detail between adjacent atoms, but instead pick out the atoms and sites that are accessible at the boundary of the configuration.

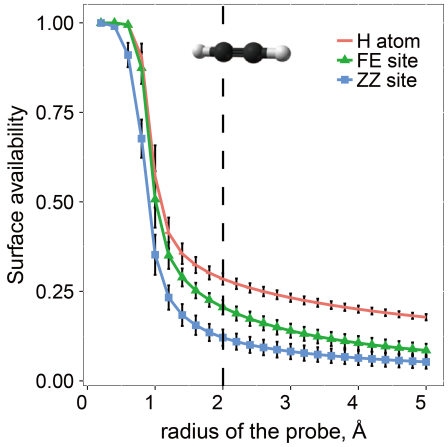

Figure 4: *Surface availabilities of hydrogen atoms, FE and ZZ sites of a liquid-like coronene$_{500}$ cluster at 575 K as a function of the probe size. The error bars are the standard deviations computed from 100 different samples of the configuration. The size of an acetylene molecule is highlighted by the dashed line.*

3.2 Temperature dependence of the surface availability

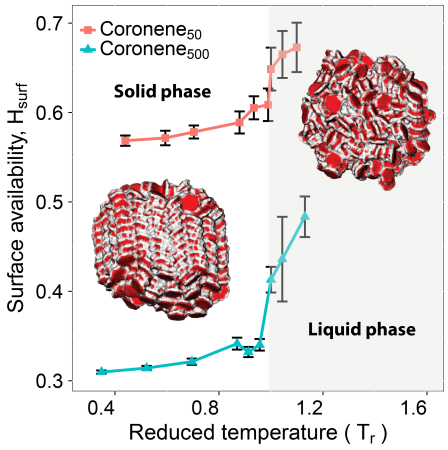

Figure 5: *Surface availability of hydrogen atoms on coronene$_{50}$ and coronene$_{500}$ clusters as a function of the reduced temperature. The radius of probe is 1.2 Å which is analogous to that of a hydrogen atom. The configurations of the coronene$_{500}$ cluster at $T_r = 0.96$ (left) and 1.0 (right) are also embedded on the plot. The melting point of both coronene$_{50}$ and coronene$_{500}$ are taken from Chen et al. [8] and are 455 K and 575 K respectively. The error bars are the standard deviations computed from 100 different samples of the configuration.*

The surface availability of hydrogen atom on coronene$_{50}$ and coronene$_{500}$ clusters have been examined to illustrate the impact of temperature (Fig. 5). The results are reported in terms of the reduced temperature T$_r$, defined as $T_{\mathrm{r}} = T_{\mathrm{actual}}/T_{\mathrm{melting\ point}}$. The melting points of individual nano-cluster were taken from previous work [8]. The maximum reduced temperature in this work was 1.13 or $T_{\mathrm{actual}} = 650$ K for a coronene$_{500}$ cluster [8].

At higher temperatures these particles are highly mobile and favour thermal dissociation for $T_r \geq 1.1$ [29]. However, this does not indicate that the findings in this work are irrelevant to soot particles, where it is common for soot to exist at 1500 K or above. It is well accepted that soot particles appear as solid-like configurations even within the center of a flame. This suggests the soot particles form at T_r less than 1.0, which is a region that is accessible using coronene and pyrene clusters.

Fig. 5 shows that the particles at higher temperatures yield higher surface availabilities, and that there is a pronounced increase in the surface availability as the particles melt. Similar observations are found for both FE and ZZ sites. Not surprisingly, the increase in surface availability as the particles melt is accompanied by a significant change in the particle morphology. Previous work [8] has demonstrated that the solid particles are composed of multiple parallel stacks of PAHs with clear surface edges, whilst the melted particles are composed of small stacks of three to seven PAHs and exhibit very irregular surfaces. The ordered crystal-like morphology of the solid particles limit the access of gaseous species and consequently, the number of surface hydrogen, FE and ZZ sites is limited. In contrast, the irregular surface of the melted particles allow a higher exposure to gaseous species and enhance the surface availabilities of hydrogen atoms, FE and ZZ sites. However, this observation disagrees with common estimates of the parameter α, which is believed to decrease with temperature [1, 12, 34].

3.3 Particle size dependence of the surface availability

In a recent expression of the parameter α [1], the parameter is not only temperature dependent, but also particle size dependent. Similarly, Fig. 6 shows the surface reactivities of different-sized pyrene and coronene clusters at their melting points using a probe representing an acetylene molecule. It is found that the surface availability reduces with increasing particle size, and follows a linear relation with reciprocal size. This observation is consistent with that of Appel et al. [1]. The surface availability of the coronene clusters is approximately 0.05-0.1 higher than that of the pyrene clusters. From the slope of the fitted lines, we can extract information about the decay rates of these surface properties. The decay rate of the FE and ZZ sites is approximately 0.75 and 0.45 times of that of hydrogen atoms. The lower availability of ZZ versus FE sites is attributed to the concave structure of the ZZ sites, where the carbon atom at the centre of the concave region is expected to be less accessible than the equivalent atom in a FE site.

On Fig. 6, The surface availabilities of hydrogen atoms, FE and ZZ sites lie in the ranges 0.2-0.6, 0.2-0.4 and 0.1-0.3 respectively for nascent soot, interpreted as particles less than 10 nm in diameter. The surface availabilities are significantly lower (and well below 0.1) for mature soot, interpreted as particles greater than 50 nm. The surface availability of the hydrogen atoms can be interpreted as the upper bound of α in the context of the HACA mechanism, where hydrogen abstraction is believed to initiate the surface reactions. This work offers a rationale to guide the selection of the parameter α in flame modelling. For instance, the value of α from a set of laminar premixed flames [35] is always greater than 0.4 when using PREMIX [15] in which the α expression is that of Appel et al. [1]. In these flames, the largest and moderate-sized particles are approximately 50 nm and 10 nm in diameter [35]. However, using the correlation for the coronene cluster from Fig. 6a,

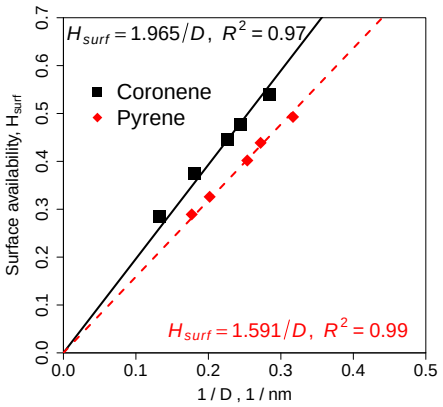

(a) *H atom*

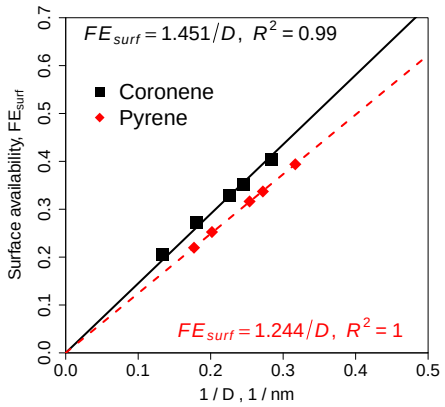

(b) *FE site*

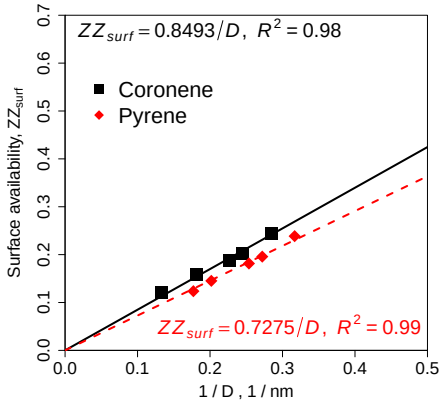

(c) *ZZ site*

Figure 6: *Surface availabilities of hydrogen atoms, FE and ZZ sites on pyrene and coronene clusters at $T_r = 1.0$ as a function of the reciprocal of particle diameter. The probe radius is 2.0 Å which is analogous to that of an acetylene molecule. The equation of the straight lines of best fit and the corresponding R^2 value are shown at the top of each plot for the coronene and the bottom of each plot for the pyrene.*

the upper bound of α should be 0.04 and 0.2 for the largest and moderate-sized particles respectively. Thus, an overestimation of the surface reactivity of large particles is clearly suggested. More recently, Dworkin et al. [11] optimised the parameter α by fitting the predicted maximum soot volume fraction to experimental data for a co-flow ethylene/air non-premixed flame. It was found that the experimental trends of the soot fraction were successfully captured using a constant α as small as 0.078. Saffaripour et al. [25] further proposed an alpha value of 0.0045 to improve the quality of their model. Compared with findings in this work, both values lie below the suggested upper bound of parameter α. In summary, the upper bound of the parameter α for acetylene-dominated processes can be used to guide the fidelity of predictions from numerical simulations where the surface

processes dominate the mass growth of the soot.

3.4 Surface pockets

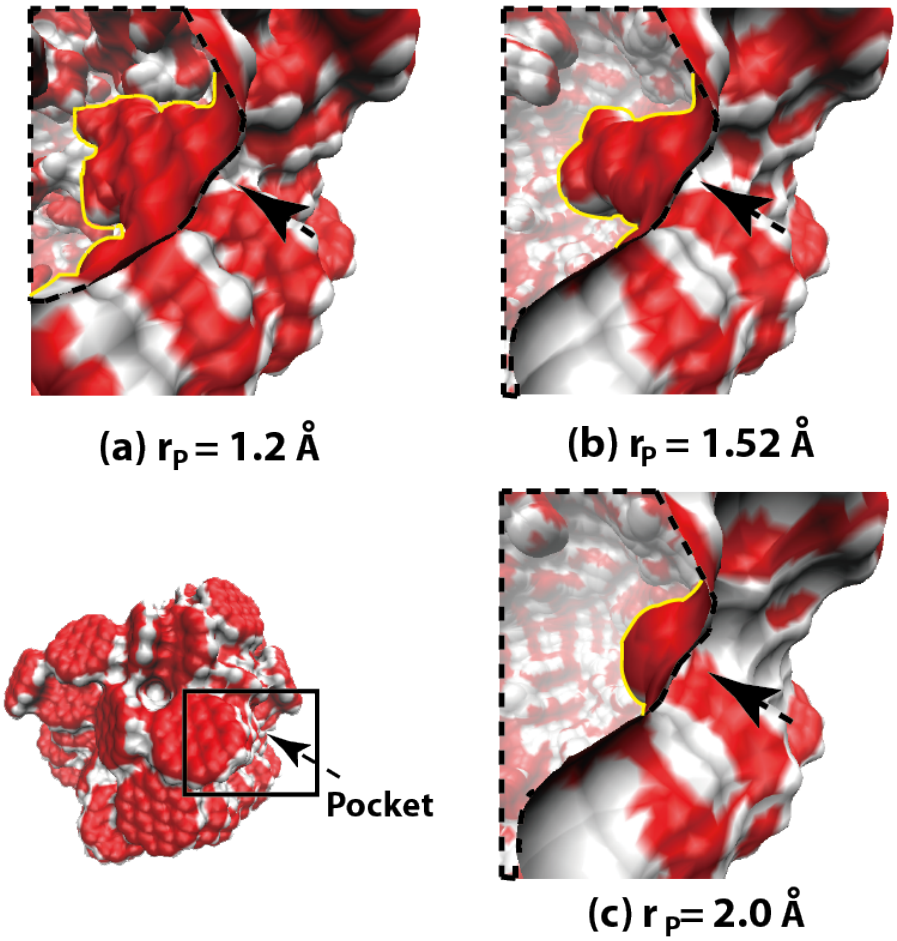

Figure 7: *Side view snapshots of a pocket on a liquid-like coronene$_{100}$ cluster using a probe of radius r_p = 1.2 Å (a), 1.52 Å (b) and 2.0 Å (c) at 500 K. The red color represents the contribution of the carbon atoms, whilst the white color represents the contribution of the hydrogen atoms to the SES. The black arrows point to the location of the pocket on the configuration. The black dash lines highlight the sections of the configuration, and the yellow solid lines outline the extent of the pockets beyond the boundary of the configuration.*

To investigate explicitly the surface pockets, one particular pocket on a coronene$_{100}$ cluster at 500 K was carefully examined using different probe sizes ranging from 1.2 Å to 2.0 Å (Fig. 7). The existence of pockets in the coronene$_{100}$ clusters supports the proposition that it is feasible for small gaseous molecules to penetrate inside a particle. As outlined by the yellow solid line, the size of the pocket decreases with the increase in the probe size. This supports the observation that a small probe gains a larger accessibility within a configuration, whilst the accessibility that of a large probe is limited. It is also noted that the depth

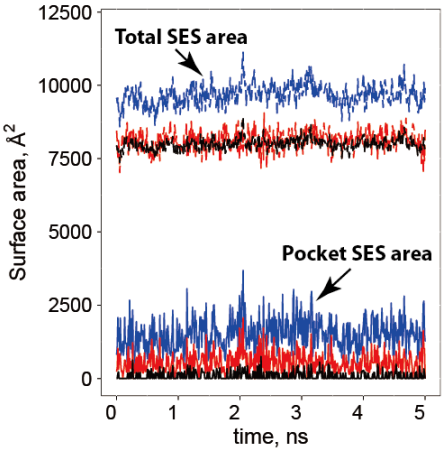

Figure 8: *Evolution of pocket SES area and total SES area of a liquid-like coronene$_{100}$ cluster at $T_r = 1.0$ (500 K) using a probe of radius $r_p = 1.2$ Å (blue), 1.52 Å (red) and 2.0 Å (black).*

of the pockets vary with the size of the probe. The depths of the pockets in Fig. 7 are approximately 1.5 nm (Fig. 7a), 1.1 nm (Fig. 7b) and 0.4 nm (Fig. 7c). Compared to the average 0.35 nm layer separation of a PAH stack [31], this pocket provides a pathway for an oxygen molecule to access PAHs located up to 3 layers deep within a PAH stack on the surface whilst even an acetylene molecule can access at least 2 layers deep. The surface reactions are not limited to the boundary of the configuration but also regions beyond the boundary of a particle. Fig. 8 shows the transient evolution of the pocket and total SES area of the coronene$_{100}$ clusters. Both the pocket SES area and the total SES area fluctuate around an average value. The fluctuations are caused by molecular rearrangements and indicate that individual pockets have a short lifetime and continuously appear and disappear. Although the lifetime of an individual pocket is short, it still provides a possible reaction pathway by which the gas-phase species can react with not only the active sites on the boundary of a configuration but also sites inside the configuration.

4 Conclusion

We propose a scheme to characterise surface atoms based on the solvent-excluded surface and demonstrate how to extract the surface properties from a molecular arrangement using this scheme. The availabilities of the surface active atoms and sites including hydrogen atoms, FE and ZZ sites are investigated to shed a light on the surface reactivity of homogenous pyrene and coronene clusters with diameters from about 3 to 8 nm. The accessibility of the active sites on the clusters vary with gas-phase species. Small species usually have a high accessibility while the accessibility of large species is limited. The surface availability also shows a temperature and particle size dependence. Higher temperatures lead to a higher exposure of the molecular surface. Further, the surface availability is significantly enhanced when crossing the melting point because of the change in the particle morphology. The upper bound of the parameter α for acetylene-based processes is es-

timated, and shown to decrease with increasing particle size following a linear relation with reciprocal size. By exploring one particular pocket on the surface of a coronene$_{100}$ cluster with different probe sizes, it is found that both oxygen and acetylene molecules are able to access certain regions beyond the boundary of a particle. It is also noted that the lifetime of pockets is very short, but this fact does not preclude the possibility that gas-phase species can react with active sites buried inside a configuration.

Acknowledgements

This work was supported by the Singapore National Research Foundation under its Campus for Research Excellence And Technological Enterprise (CREATE) programme. The authors also acknowledge financial support from Shell Research Ltd. and from Churchill College, Cambridge.

References

[1] J. Appel, H. Bockhorn, and M. Frenklach. Kinetic modeling of soot formation with detailed chemistry and physics: Laminar premixed flames of C_2 hydrocarbons. *Combustion and Flame*, 121:122–136, 2000. doi:10.1016/S0010-2180(99)00135-2.

[2] M. Balthasar, F. Mauss, A. Knobel, and M. Kraft. Detailed modeling of soot formation in a partially stirred plug flow reactor. *Combustion and Flame*, 128(4):395–409, 2002. doi:10.1016/S0010-2180(01)00344-3.

[3] A. Bondi. van der Waals Volumes and Radii. *The Journal of Physical Chemistry*, 68(3):441–451, 1964. doi:10.1021/j100785a001.

[4] M. S. Celnik, A. Raj, R. H. West, R. I. A. Patterson, and M. Kraft. An aromatic site description of soot particles. *Combustion and Flame*, 155(1-2):161–180, 2008. doi:10.1016/j.combustflame.2008.04.011.

[5] M. S. Celnik, M. Sander, A. Raj, R. H. West, and M. Kraft. Modelling soot formation in a premixed flame using an aromatic-site soot model and an improved oxidation rate. *Proceedings of the Combustion Institute*, 32(1):639–646, 2009. doi:10.1016/j.proci.2008.06.062.

[6] D. Chen, Z. Zainuddin, E. Yapp, J. Akroyd, S. Mosbach, and M. Kraft. A fully coupled simulation of PAH and soot growth with a population balance model. *Proceedings of the Combustion Institute*, 34(1):1827–1835, 2013. doi:10.1016/j.proci.2012.06.089.

[7] D. Chen, T. Totton, J. Akroyd, S. Mosbach, and M. Kraft. Phase change of polycyclic aromatic hydrocarbon clusters by mass addition. 2013, submitted.

[8] D. Chen, T. S. Totton, J. W. Akroyd, S. Mosbach, and M. Kraft. Size-dependent melting of polycyclic aromatic hydrocarbon nanoclusters: A molecular dynamics study. *Carbon*, 67(0):79–91, 2014. doi:http://dx.doi.org/10.1016/j.carbon.2013.09.058.

[9] M. Connolly. Solvent-accessible surfaces of proteins and nucleic acids. *Science*, 221(4612):709–713, 1983. doi:10.1126/science.6879170.

[10] M. Connolly. Analytical molecular surface calculation. *Journal of Applied Crystallography*, 16(5):548–558, 1983. doi:10.1107/S0021889883010985.

[11] S. B. Dworkin, Q. Zhang, M. J. Thomson, N. A. Slavinskaya, and U. Riedel. Application of an enhanced PAH growth model to soot formation in a laminar coflow ethylene/air diffusion flame. *Combustion and Flame*, 158(9):1682–1695, 2011. doi:10.1016/j.combustflame.2011.01.013.

[12] M. Frenklach and H. Wang. Detailed modeling of soot particle nucleation and growth. *Symposium (International) on Combustion*, 23(1):1559–1566, 1991. doi:10.1016/S0082-0784(06)80426-1.

[13] S. Henrich, O. M. H. Salo-Ahen, B. Huang, F. F. Rippmann, G. Cruciani, and R. C. Wade. Computational approaches to identifying and characterizing protein binding sites for ligand design. *Journal of Molecular Recognition*, 23(2):209–219, 2010. doi:10.1002/jmr.984.

[14] A. Kazakov, H. Wang, and M. Frenklach. Detailed modeling of soot formation in laminar premixed ethylene flames at a pressure of 10 bar. *Combustion and Flame*, 100:111–120, 1995. doi:10.1016/0010-2180(94)00086-8.

[15] R. J. Kee, K. Grcar, M. D. Smooke, and J. A. Miller. Premix: A fortran program for modelling steady laminar one-dimensional premixed flames. Technical Report UC-4 SAND85-8240, SANDIA National Laboratories, 1985.

[16] M. Kholghy, M. Saffaripour, C. Yip, and M. J. Thomson. The evolution of soot morphology in a laminar coflow diffusion flame of a surrogate for Jet A-1. *Combustion and Flame*, 160(10):2119–2130, 2013. doi:http://dx.doi.org/10.1016/j.combustflame.2013.04.008.

[17] C. Kim, A. El-Leathy, F. Xu, and G. Faeth. Soot surface growth and oxidation in laminar diffusion flames at pressures of 0.1-1.0 atm. *Combustion and Flame*, 136 (1-2):191–207, 2004. doi:http://dx.doi.org/10.1016/j.combustflame.2003.09.017.

[18] B. Lee and F. Richards. The interpretation of protein structures: Estimation of static accessibility. *Journal of Molecular Biology*, 55(3):379–400, 1971. doi:http://dx.doi.org/10.1016/0022-2836(71)90324-X.

[19] J. Liang, C. Woodward, and H. Edelsbrunner. Anatomy of protein pockets and cavities: Measurement of binding site geometry and implications for ligand design. *Protein Science*, 7(9):1884–1897, 1998. doi:10.1002/pro.5560070905.

[20] R. I. A. Patterson, J. Singh, M. Balthasar, M. Kraft, and W. Wagner. Extending stochastic soot simulation to higher pressures. *Combustion and Flame*, 145(3):638–642, 2006. doi:10.1016/j.combustflame.2006.02.005.

[21] A. Raj, M. Celnik, R. Shirley, M. Sander, R. Patterson, R. West, and M. Kraft. A statistical approach to develop a detailed soot growth model using PAH characteristics. *Combustion and Flame*, 156(4):896–913, 2009. doi:10.1016/j.combustflame.2009.01.005.

[22] A. Raj, P. L. Man, T. S. Totton, M. Sander, R. A. Shirley, and M. Kraft. New polycyclic aromatic hydrocarbon (PAH) surface processes to improve the model prediction of the composition of combustion-generated PAHs and soot. *Carbon*, 48 (2):319–332, 2010. doi:10.1016/j.carbon.2009.09.030.

[23] F. M. Richards. Areas, volumes, packing, and protein structure. *Annual Review of Biophysics and Bioengineering*, 6(1):151–176, 1977. doi:10.1146/annurev.bb.06.060177.001055.

[24] T. J. Richmond. Solvent accessible surface area and excluded volume in proteins: Analytical equations for overlapping spheres and implications for the hydrophobic effect. *Journal of Molecular Biology*, 178(1):63–89, 1984. doi:http://dx.doi.org/10.1016/0022-2836(84)90231-6.

[25] M. Saffaripour, M. Kholghy, S. Dworkin, and M. Thomson. A numerical and experimental study of soot formation in a laminar coflow diffusion flame of a Jet A-1 surrogate. *Proceedings of the Combustion Institute*, 34(1):1057–1065, 2013. doi:http://dx.doi.org/10.1016/j.proci.2012.06.176.

[26] M. Sander, R. I. Patterson, A. Braumann, A. Raj, and M. Kraft. Developing the PAH-PP soot particle model using process informatics and uncertainty propagation. *Proceedings of the Combustion Institute*, 33(1):675–683, 2011. doi:10.1016/j.proci.2010.06.156.

[27] M. F. Sanner, A. J. Olson, and J. C. Spehner. Reduced surface: An efficient way to compute molecular surfaces. *Biopolymers*, 38(3):305–320, 1996. doi:10.1002/(SICI)1097-0282(199603)38:3<305::AID-BIP4>3.0.CO;2-Y.

[28] M. Schenk, S. Lieb, H. Vieker, A. Beyer, A. Gölzhäuser, H. Wang, and K. Kohse-Höinghaus. Imaging nanocarbon materials: Soot particles in flames are not structurally homogeneous. *Chemical physics and physical chemistry*, 14(14):3248–3254, 2013. doi:10.1002/cphc.201300581.

[29] M. Schmidt, A. Masson, and C. Bréchignac. Coronene cluster experiments: Stability and thermodynamics. *International Journal of Mass Spectrometry*, 252(2):173–179, 2006. doi:10.1016/j.ijms.2005.10.015.

[30] B. K. Shoichet, I. D. Kuntz, and D. L. Bodian. Molecular docking using shape descriptors. *Journal of Computational Chemistry*, 13(3):380–397, 1992. doi:10.1002/jcc.540130311.

[31] T. S. Totton, D. Chakrabarti, A. J. Misquitta, D. J. Wales, and M. Kraft. Modelling the internal structure of nascent soot particles. *Combustion and Flame*, 157(5):909–914, 2010. doi:10.1016/j.combustflame.2009.11.013.

[32] L. G. Vincent, S. Peter, and T. Pierre. Fpocket: An open source platform for ligand pocket detection. *BMC Bioinformatics*, 10:106, 2009. doi:10.1186/1471-2105-10-168.

[33] F. Xu, P. Sunderland, and G. Faeth. Soot formation in laminar premixed ethylene/air flames at atmospheric pressure. *Combustion and Flame*, 108(4):471–493, 1997. doi:http://dx.doi.org/10.1016/S0010-2180(96)00200-3.

[34] F. Xu, K. C. Lin, and G. M. Faeth. Soot formation in laminar premixed Methane/Oxygen flames at atmospheric pressure. *Combustion and Flame*, 115:195–209, 1998. doi:http://dx.doi.org/10.1016/S0010-2180(98)00017-0.

[35] B. Zhao, Z. Yang, Z. Li, M. V. Johnston, and H. Wang. Particle size distribution function of incipient soot in laminar premixed ethylene flames: Effect of flame temperature. *Proceedings of the Combustion Institute*, 30(1):1441–1448, 2005. doi:10.1016/j.proci.2004.08.104.